Account/Review for Life Chemistry

Surface-Based Nanoplasmonic Sensors for Biointerfacial Science Applications

Joshua A. Jackman,[1] **Abdul Rahim Ferhan,**[2] **and Nam-Joon Cho**[*2,3]

[1]School of Chemical Engineering, Sungkyunkwan University, Suwon 16419, Korea

[2]School of Materials Science and Engineering, Nanyang Technological University,
50 Nanyang Avenue, Singapore 639798, Singapore

[3]School of Chemical and Biomedical Engineering, Nanyang Technological University,
62 Nanyang Drive, Singapore 637459, Singapore

E-mail: njcho@ntu.edu.sg

Joshua A. Jackman
Joshua A. Jackman is an Assistant Professor in the School of Chemical Engineering at Sungkyunkwan University. He received his BS degree in Chemistry from the University of Florida and PhD degree in Materials Science and Engineering from Nanyang Technological University and was a postdoctoral scholar at the Stanford University School of Medicine. He has received fellowships from the Arnold and Mabel Beckman Foundation, National Science Foundation, and American Liver Foundation. His research interests lay at the interface of materials science and biotechnology towards developing biosensors, bioanalytical measurement platforms, and medical technologies.

Abdul Rahim Ferhan
Abdul Rahim Ferhan is a Research Fellow in the Engineering in Translational Science group in the School of Materials Science and Engineering at Nanyang Technological University. He received his BEng degree in Chemical and Biomolecular Engineering and PhD degree in Biomedical Engineering from the School of Chemical and Biomedical Engineering at Nanyang Technological University. His research focuses on the development and application of novel nanoplasmonic sensing platforms for biomedical diagnostics and fundamental investigations into biomacromolecular interaction processes.

Nam-Joon Cho
Nam-Joon Cho is a Nanyang Associate Professor in the School of Materials Science and Engineering and Principal Investigator of the Engineering in Translational Science group at Nanyang Technological University. A recipient of the National Research Foundation Fellowship, he received his PhD degree in Chemical Engineering from Stanford University and completed a postdoctoral fellowship at the Stanford University School of Medicine. His research focuses on engineering artificial lipid membrane and tissue platforms to probe biological systems, and to develop enhanced therapeutic and drug delivery options that more effectively target infectious diseases, inflammatory disorders, and cancer along with the development of pollen-based biomaterials.

Abstract

The design and application of surface-based nanoplasmonic sensors has spurred broad interest from the chemical science community, touching upon diverse topics such as plasmonics, nanoscience, surface chemistry, measurement analysis, and interfacial science. One of the most exciting areas involves taking advantage of the simple instrumental requirements and high surface sensitivity of these sensing devices to study biomacromolecules and biological nanoparticles. In this Account, we present a narrative summary describing our recent

work to explore surface-based nanoplasmonic sensors for biointerfacial science applications and outlining our perspective on possible future directions. After introducing the basic design concepts and measurement principles behind surface-based nanoplasmonic sensors, we focus on critically discussing recent application examples from our laboratory, where the high surface sensitivity of surface-based nanoplasmonic sensors proved useful for studying lipid vesicles, supported lipid bilayers, virus-like particles, proteins, and peptides. The potential of integrating surface-based nanoplasmonic sensors with other surface-sensitive measurement techniques is also discussed. Looking forward, there is excellent potential to continue using surface-based nanoplasmonic sensors for biointerfacial science applications and numerous innovation opportunities exist from fundamental and applied perspectives.

Keywords: Nanoplasmonics | Biosensors | Biointerfaces

Introduction

The interaction of light with metallic nanostructures has long played an important role in endowing materials with unique properties, such as ancient glassware that contained trace amounts of metallic nanoparticles and exhibited different colors depending on the orientation of light illumination.[1] In modern times, such properties have proven equally fascinating as we seek to understand and take advantage of the underlying physical phenomena for scientific advancement.[2] In short, light can induce the coherent oscillation of free electrons in a metallic nanostructure ("plasmons"), leading to the generation of an enhanced electromagnetic field that is useful for sensing applications.[3,4] Experimental studies on solution-phase nanoparticles with different physicochemical properties — among them, material composition, size, and shape — have refined our understanding of how nanostructures can exhibit plasmonic properties and led to the creation of the nanoplasmonics field.[5,6] Ongoing advances in nanofabrication capabilities[7] and design concepts such as nanoarchitectonics[8] have further spurred the development of surface-based nanoplasmonic sensors with highly surface-sensitive measurement capabilities.[9–12] Compared to other classes of surface-sensitive measurement techniques, nanoplasmonic sensors have several competitive advantages, including simple instrumental requirements, high environmental stability, fast response time, and label-free detection. Thus, there is great interest in surface-based nanoplasmonic sensors, and our laboratory has focused on utilizing them for biointerfacial science applications.

Surface-Based Nanoplasmonic Sensors

The development of surface-based nanoplasmonic sensors originated with depositing plasmonic metal nanoparticles onto non-metallic solid supports[13] (e.g., glass). Discrete nanoparticles can be attached to a solid support via numerous possible functionalization strategies involving noncovalent and/or covalent chemistries.[14] In comparison to solution-phase nanoparticles, a major advantage of immobilizing nanoparticles on a solid support is that the nanoparticles remain firmly attached to the solid support during biosensing experiments. Thus, surface-based nanoplasmonic sensors provide a stable measurement

platform and the acquired experimental data are focused on tracking measurement responses that occur due to biomacromolecular interaction processes such as adsorption and conformational changes without detriment from interfering factors such as nanoparticle aggregation in bulk solution.

Depending on the preparation conditions, discrete nanoparticles can be deposited on a target surface with varying surface coverages. If the deposited nanoparticles have a low surface coverage and a non-periodic, non-interacting arrangement, then the principal measurement response will arise from the localized surface plasmon resonance (LSPR) of the metal nanoparticles.[11,15] LSPR generation involves the resonant oscillation of conducting electrons that are tightly confined to the nanoparticle surface and induces an enhanced electromagnetic field in the near vicinity to the surface (decay length of the enhanced electromagnetic field is typically on the order of 10–20 nm).[3] The experiments are usually conducted in a transmission-mode configuration and the optical extinction (sum of light absorption and scattering) is characterized by a maximum-extinction wavelength that is known as the LSPR peak position, or simply λ_{max} (Figure 1).

If a biomacromolecule adsorbs onto the sensor surface, then the local refractive index will be shifted, and this typically causes an increase (red-shift) in the λ_{max} that is reported as a $\Delta\lambda_{max}$ shift. Aside from depositing nanoparticles onto a solid support, it is also possible to fabricate nanoparticles directly on a solid support, thus enabling greater control over the organizational arrangement of the nanoparticles on the surface, including density and periodicity. For example, a periodic arrangement of nanoparticles on a solid support can give rise to near- and/or far-field coupling that influences the plasmonic properties, including leading to an increase in the decay length of the enhanced electromagnetic field in some cases.[16] Such features have led researchers to begin to classify nanoplasmonic sensor performance[17–19] based on bulk sensitivity (measurement response arising from changes in the bulk refractive index of a solution media) and surface sensitivity (measurement response arising from changes in the local refractive index near a sensor surface).

In addition to nanoparticle-based sensing platforms, it is also possible to design nanohole-based sensing platforms where the
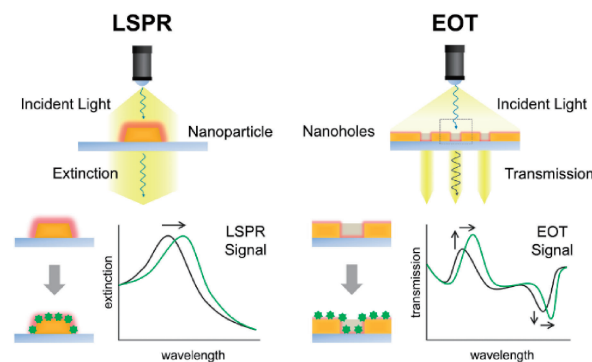

Figure 1. Surface-based nanoplasmonic sensors operating based on the localized surface plasmon resonance (LSPR) and extraordinary optical transmission (EOT) effects. Reproduced from Ref. 11 with permission from The Royal Society of Chemistry, 2017.

voids in a thin metallic film can exhibit plasmonic properties.[10,11] One of the most prominent examples involves periodic arrays of nanoholes in a thin metallic film; interaction of light with this particular type of nanostructure gives rise to extraordinary optical transmission (EOT). Specifically, when light passes through subwavelength nanoholes, the EOT effect causes greatly enhanced transmission efficiency of light at certain wavelengths.[20,21] Experimentally, the transmission spectrum is recorded and exhibits several distinct peaks related to enhanced transmission (greater intensity) along with several minima as well. Typically, all of these spectral features shift in response to a biomacromolecular adsorption event, although each one corresponds to a distinct combination of one or more plasmon modes and thus exhibits different degrees of bulk and surface sensitivities. Unraveling the details of this complex optical phenomena is ongoing and there is already strong evidence that EOT-based sensing platforms are useful for biosensing applications[22,23] as well. In most cases, researchers have focused on tracking spectral features with the highest bulk sensitivities [thus, they are commonly referred to as "nanohole SPR" instruments in reference to conventional surface plasmon resonance (SPR) instruments that have high bulk refractive index sensitivity but lower surface sensitivity] although we and others have started to look at other spectral features that are sensitive to different regions of the nanohole geometry and have different surface sensitivities, as discussed below. There is also interest in exploring the plasmonic properties of individual nanoholes[24] and short-range ordered nanoholes,[25] both of which have useful sensing purposes as well.

Inherently, the fabrication of metallic nanoparticle- and nanohole-based arrays on non-metal supporting substrates creates sensing platforms with heterogenous material properties and developing functionalization strategies to homogenize the material properties of the contacting sensor surface is advantageous for biointerfacial science applications. Towards this goal, there has been tremendous progress in conformally coating nanoplasmonic sensing platforms with thin layers of a dielectric film such as an oxide layer in order to present a uniform material surface, diversify the range of surface chemistry possibilities, and impart high stability to the underlying nanoplasmonic transducers, leading to the development of the indirect nanoplasmonic sensing (INPS) concept[26] (Figure 2). Importantly, the dielectric layer is sufficiently thin so that the enhanced electromagnetic field can penetrate through the layer

and biosensing interactions occurring at the dielectric-liquid interface can be detected with high sensitivity.[27,28]

The combination of these sensing features — both the plasmonic and materials chemistry aspects — has proven highly beneficial to utilize surface-based nanoplasmonic sensor platforms for biointerfacial science applications, as demonstrated in pioneering works revealing new insights into the conformational properties of biomacromolecules (e.g., proteins[29]) and biological nanoparticles (e.g., lipid vesicles[30]). Compared to conventional SPR biosensors involving propagating surface plasmons on thin metal films, surface-based nanoplasmonic sensors have several compelling features, including simpler optical setup, greater environmental stability (i.e., relatively low bulk sensitivity reduces noise arising from environmental changes such as minor temperature fluctuations), and higher surface sensitivity.[31,32] Coming from a materials science perspective, we were intrigued by these bioanalytical measurement possibilities and sought to explore how surface-based nanoplasmonic sensors can be useful for studying a wide range of biointerfacial science topics, along with laying the groundwork towards establishing a quantitative framework to interpret measurement data and to shed light on mechanistic aspects of biomacromolecular interaction processes. In the following sections, we critically discuss different examples from our laboratory where surface-based nanoplasmonic sensors provided new insights into biomacromolecular interaction processes.

Lipid Vesicle Adsorption

Our first nanoplasmonic sensing project involved studying lipid vesicle adsorption onto oxide film-coated gold nanodisk arrays. The gold nanodisks were fabricated on a glass surface via hole-mask colloidal lithography and used either as-is or the entire sensor surface was subsequently coated with a conformal layer of titania or silicon nitride. Upon oxygen plasma treatment, the top layer of the silicon nitride layer becomes converted into a silica overlayer and we refer to the surface accordingly since the outermost layer is the contacting surface for adsorption experiments. Thus, we investigated vesicle adsorption onto three types of surfaces: (i) bare gold nanodisks on a glass support, (ii) a titania-coated surface containing embedded gold nanodisks; and (iii) a silica-coated surface containing embedded gold nanodisks.[33] From a materials science perspective, the results were intriguing because we discovered that adsorbed vesicles ruptured to form a supported lipid bilayer (SLB) coating on a glass surface while vesicles appeared to adsorb but not rupture on top of the bare gold nanodisks. The resulting lipid nanoarchitecture was comprised of a SLB coating interspersed with adsorbed lipid vesicles on top of the nanodisks, a particularly unique configuration that highlighted the potential of merging nanofabrication with the molecular self-assembly of biological macromolecules. Likewise, adsorbed vesicles ruptured to form an SLB coating on the silica-coated surfaces while the adsorbed vesicles remained intact on the titania-coated surface, forming a close-packed layer (Figure 3a).

Aside from the interesting nanoarchitectures of the phospholipid assemblies, we felt there was untapped potential for studying quantitative aspects of lipid vesicle adsorption with this label-free nanoplasmonic sensing platform so we decided
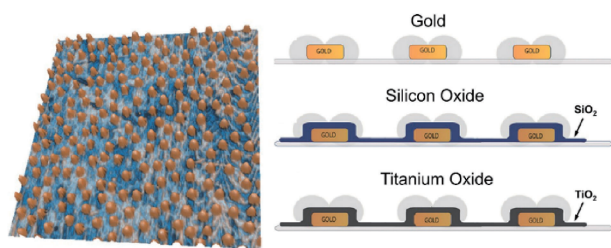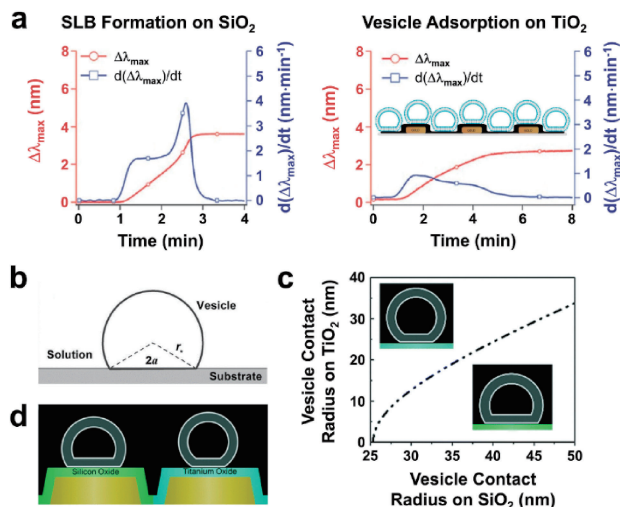

Figure 2. Nanoplasmonic sensing platform architectures consisting of bare gold nanodisks on a glass support, by themselves or coated with an oxide layer as part of the INPS concept. Reproduced from Ref. 33 with permission from Wiley-VCH, 2014.

Figure 3. (a) Supported lipid bilayer formation on silica versus intact vesicle adsorption on titania. Reproduced from Ref. 33 with permission from Wiley-VCH, 2014. (b) Deformation of an adsorbed vesicle represented as a truncated sphere. Reproduced from Ref. 38 with permission from American Chemical Society, 2015. (c) Calculated variation in contact radius of adsorbed vesicles on silica-versus titania-coated surfaces. (d) Adsorbed vesicles undergo greater substrate-induced deformation on silica surfaces, as compared to titania surfaces. Reproduced from Ref. 36 with permission from The Royal Society of Chemistry, 2016.

to explore further in this direction. The embedded gold nanodisks exhibited plasmonic properties and LSPR generation created an enhanced electromagnetic field that slightly extends beyond the sensor surface and is sensitive to changes in the local dielectric environment. Such changes affect the LSPR resonance conditions and can be detected as maximum-extinction wavelength shifts as a function of measurement time. Together with Professor Vladimir Zhdanov of the Russian Academy of Sciences, we developed analytical models to understand how LSPR measurement responses would be affected by vesicle adsorption, taking into account aspects such as diffusion-limited adsorption kinetics and adsorbate-related LSPR physics (Figure 3b).[34] We applied these models to experimentally study the effects of vesicle concentration and vesicle size on vesicle adsorption kinetics. For ∼60-nm diameter lipid vesicles, we discovered that greater levels of saturation coverage were achieved with higher bulk lipid concentrations, signaling that the adsorption time scale is important for achieving optimal packing densities. We also discovered that the time-derivative of the LSPR measurement response provided insight into the diffusion-limited adsorption rate, a feature which we rigorously applied for quantitative analysis as explained below. Another key finding was that the LSPR measurement approach was particularly well-suited for vesicles of less than 100 nm diameter while more complex measurement responses were observed with larger vesicles due to extensive deformation and correlations with the location of gold nanodisks.

While the LSPR measurement response provided a useful marker of vesicle adsorption kinetics, we wanted to further

understand how the deformation of adsorbed vesicles influences the measurement response. Based on the distance-dependent decay of the enhanced electromagnetic field, we derived general equations to describe how the deformation of an adsorbed vesicle would affect the LSPR measurement response at low surface coverage (the initial rate of change in the LSPR signal) and at high surface coverage (the net shift at saturation). An important aspect of this work is that the decay length is typically around 10–20 nm, which is comparable to the length scale of lipid vesicles (50–100 nm diameter). As such, the deformation of an adsorbed vesicle will have a significant effect on the amount of lipid material that is within the high-intensity field region. By contrast, if the decay length were an order of magnitude longer (∼200 nm, as is typical with conventional SPR biosensors), it would be less sensitive to the deformation of adsorbed vesicles. Following this approach, we have been able to compare the deformation of adsorbed vesicles under different environmental conditions. In one particular example, we examined how the presence of divalent cations affects the deformation of adsorbed vesicles on titania and silica surfaces and discovered that cations promote increased deformation of adsorbed vesicles in the order of $Ca^{2+} > Mg^{2+} > Sr^{2+}$.[35]

In general, we have found that measuring the initial rate of change in the LSPR signal provides a reliable indicator of vesicle deformation. Vesicle adsorption is a diffusion-limited process that depends on the bulk hydrodynamics of vesicles in solution. If all the relevant parameters are fixed (*i.e.*, solution viscosity, experimental temperature, vesicle size, vesicle concentration), the initial rate of change in the LSPR signal will vary depending on the strength of the vesicle-substrate interaction. In other words, if the vesicle-substrate interaction is stronger, then an adsorbed vesicle will be more deformed and contribute to a larger measurement response. As such, the rate of change in the LSPR signal would be greater with increased, substrate-induced deformation of adsorbing vesicles. In addition to adjusting environmental conditions, we also applied this approach to compare the deformation of adsorbed vesicles on silica- and titania-coated sensor surfaces (Figure 3c).[36] A subtle distinction in this case is that the two substrates have different surface sensitivities so experimental controls and finite-difference time-domain (FDTD) simulations were conducted to establish a normalization procedure so that measurement data collected on the two substrates could be directly compared. Based on this approach, we determined that adsorbed vesicles undergo greater substrate-induced deformation on silica surfaces, as compared to titania surfaces (Figure 3d). This finding provided the first direct experimental evidence comparing the deformation of adsorbed vesicles on two different surfaces and is consistent with current knowledge about lipid-substrate interactions on the two surfaces.

In later work, we qualified this measurement approach by comparing how ion-induced osmotic pressure gradients affect the deformation of flexible, fluid-phase lipid vesicles and rigid, gel-phase lipid vesicles.[37] While changing the osmotic pressure across fluid-phase lipid vesicles affected the LSPR measurement response due to different extents of substrate-induced deformation, there was no change in the LSPR measurement response when studying the adsorption of gel-phase lipid

vesicles under different osmotic pressure conditions. This experimental series provided strong validation to support that the LSPR sensing approach is detecting varying extents of vesicle deformation on the sensor surface. It has also been possible to study the deformation of adsorbed vesicles at different temperatures, which is especially useful for comparing adsorption kinetics when vesicles are in the fluid-phase versus gel-phase states.[38] In such cases, the key experimental objective is to investigate vesicle adsorption above and below the gel-to-fluid phase transition temperature of lipids used in the vesicle preparation. Following this approach, it was possible to unravel how membrane phase-dependent lipid packing density affects the measurement response along with seeing how temperature can either promote or inhibit deformation of adsorbed vesicles depending on the experimental system under consideration. From a measurement perspective, these temperature-dependent LSPR studies also highlighted the benefits of high surface sensitivity and relatively low bulk sensitivity because this combination facilitates stable operating conditions without temperature-related fluctuation effects.

Spatial Proximity Sensing

The measurement principle in the aforementioned examples was based on the mismatch between the size of adsorbed vesicles ($\sim$50–80 nm diameter) and the decay length of the LSPR-amplified electromagnetic field ($\sim$10–20 nm). Specifically, a portion of an adsorbed vesicle is within the decay length, while another portion is outside the decay length. If an adsorbed vesicle is more deformed, then the lipid mass is, on average, in a region of high field intensity, resulting in a larger measurement response. To expand on this concept, we wanted to further investigate whether LSPR sensors could be applied to probe the lipid membrane geometry of nanoscale thin films that are fully within the decay length of the enhanced electromagnetic field.

To address this question, we fabricated conformal, two-dimensional SLBs on silica-coated sensor surfaces.[39] An SLB is comprised of a single lipid bilayer with a thickness on the order of 4 nm, and thus it is a useful model system for this purpose. Notably, a typical SLB on a silica surface is separated from direct contact with the silica substrate by a thin layer of water molecules ($\sim$1 nm thickness) and the exact separation distance depends on the bilayer-substrate interaction energy. We hypothesized that by varying the bilayer-substrate interaction energy, we could adjust the separation distance and detect changes in the spatial proximity of an SLB based on the LSPR measurement response. Experimentally, we controlled the membrane surface charge by adjusting the molar ratio of zwitterionic and cationic phospholipid membranes within the SLB (Figure 4a). Since the silica surface was negatively charged under the solution conditions, the bilayer-substrate separation distance was slightly tuned depending on the magnitude of the electrostatic force. Using a reflection-mode LSPR measurement setup, we identified that the LSPR measurement response for SLB formation was larger when there was a smaller separation distance between the SLB and silica surface (Figure 4b). This finding was confirmed by simultaneous quartz crystal microbalance-dissipation (QCM-D) measurements and also agreed well with theoretical calculations. The
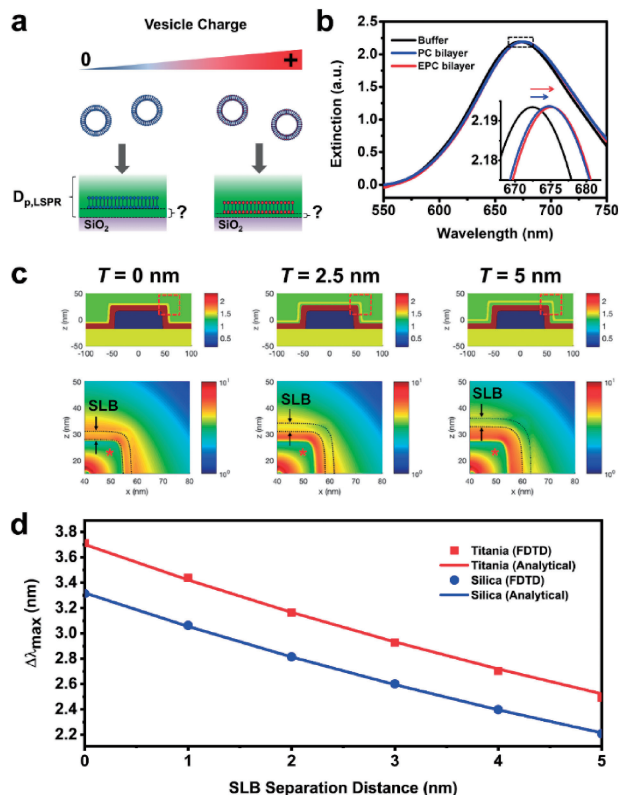

Figure 4. (a) SLB on a silica-coated substrate at different distances from the sensor surface. (b) Different degrees of LSPR $\Delta\lambda_{max}$ shifts depending on SLB distance from the sensor surface. Reproduced from Ref. 39 with permission from American Chemical Society, 2017. (c) Refractive index distributions (top) and FDTD simulations of the electric field distributions (bottom) for SLB-coated sensing platforms, with bilayer-substrate separation distances of 0, 2.5 and 5.0 nm. (d) Relationship between LSPR $\Delta\lambda_{max}$ shifts and SLB separation distance for titania- and silica-coated sensor surfaces according to FDTD simulation results and analytical calculations. Reproduced from Ref. 40 with permission from American Chemical Society, 2018.

experimental results supported that LSPR sensors can be sensitive to a sub-1 nm variation in lipid membrane conformational properties, demonstrating a higher performance level than what was previously understood to be possible.

We proceeded to next translate this measurement principle into a nanoplasmonic ruler strategy to measure the absolute separation distance between an SLB and the sensor surface.[40] In collaboration with Professor Jiří Homola's group at the Czech Academy of Sciences, we performed FDTD simulations in order to understand how the presence of an SLB coating affected the plasmonic properties of the sensing platform. The presence of multiple dielectric films on top of the gold nanodisk array, namely the oxide film layer (silica or titania) and SLB coating, gave rise to a non-monotonic field decay behavior. Thus, we extended the FDTD simulations to estimate how the SLB-substrate separation distance influences the maximum-extinction LSPR wavelength (Figure 4c), leading to the development of a model relating the LSPR measurement

response to the SLB separation distance (Figure 4d). We applied the analytical model to measure the absolute separation distance of SLBs on silica and titania surfaces. The measurements were conducted using a transmission-mode LSPR measurement setup. While SLBs were tightly coupled to silica surfaces with short separation distances on the order of 0.2 nm, the SLB separation distance was significantly larger on titania surfaces, with values around 1.2 nm. These values indicated that bilayer-substrate interactions are stronger on silica surfaces, which agreed well with literature reports and demonstrated the promise of this sensing approach.

In addition to measuring bilayer-substrate separation distances, LSPR-based spatial proximity experiments have also been useful for studying nanoparticle-membrane interactions.[41] When solution-phase silica nanoparticles were added to an SLB-coated nanodisk array, we observed monotonic adsorption of the negatively charged nanoparticles onto a zwitterionic SLB. In marked contrast, when the same nanoparticles were added to a positively charged SLB, we observed not only nanoparticle adsorption but also lipid transfer from the SLB to the nanoparticle surface. The latter process was detected by the change in spatial proximity of lipid molecules from near the sensor surface (in the SLB) to a region farther away (on the adsorbed silica nanoparticles), as indicated by a decrease in the LSPR-tracked nanoparticle adsorption rate. Lipid transfer in the case of positively charged SLBs only was attributed to attractive electrostatic interactions between positively charged lipid molecules and negatively charged silica nanoparticles.

Protein Adsorption

Protein adsorption is a broadly important subject that relates to biocompatible coatings, fouling, and surface passivation among a wide range of applications. Central to all these applications is the phenomenon that protein molecules become denatured in the adsorbed state and characterizing adsorption-related denaturation is experimentally challenging. This challenge is particularly evident when studying temperature-dependent protein adsorption, especially at high temperatures that are used in industrial settings. At a fundamental level, we were also interested in studying protein adsorption at different temperatures because protein folding is a thermally activated process and suspected that there might be a relationship between the folding of a protein molecule in bulk solution and how that protein molecule adsorbs and denatures on a material surface.

As a first step, we investigated the temperature-dependent adsorption and denaturation of bovine serum albumin (BSA) protein on a silica-coated gold nanodisk array (Figure 5a).[42]

The temperature range was varied up to 80 °C, in 10 °C increments, and we first validated that the measurement baseline in buffer conditions remains stable throughout this range. With increasing temperature, there was only a slight increase in the signal noise, without detriment to the sensing performance. Following this measurement approach, we discovered that adsorbing protein monomers undergo greater substrate-induced denaturation with increasing temperature up to ~50 °C (Figure 5b). Importantly, solution-phase biophysical measurements further supported that there was a direct relationship between the degree of reversible protein unfolding in the
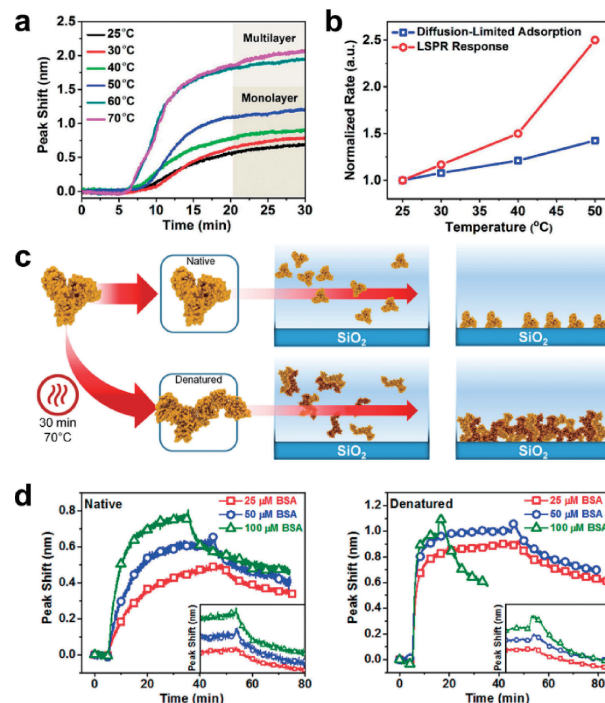

Figure 5. (a) LSPR $\Delta\lambda_{max}$ shift as a function of time for temperature-dependent BSA protein adsorption onto a silica-coated gold nanodisk array. (b) Comparison of the normalized maximum rate of change in the LSPR signal arising from BSA protein adsorption and deformation ($\partial\Delta\lambda_{max}/\partial t$) based on data from panel (a) and the normalized rate of diffusion-limited adsorption alone. Reproduced from Ref. 42 with permission from American Chemical Society, 2017. (c) Native BSA adsorption as monomers versus denatured BSA adsorption as oligomers. (d) LSPR $\Delta\lambda_{max}$ shifts as a function of time recorded for native and denatured BSA adsorption onto silica-coated surfaces. Reproduced from Ref. 43 with permission from American Chemical Society, 2018.

bulk solution and the extent of protein denaturation in the adsorbed state. On the other hand, at higher temperatures (~60 °C and higher), adsorbing proteins already underwent irreversible conformational changes in the bulk solution and protein oligomers adsorbed in this case (Figure 5c).[43] While protein adsorption at solid-liquid interfaces has long been studied by numerous types of surface-sensitive measurement techniques, the LSPR measurement strategy had a unique combination of high surface sensitivity and excellent temperature stability that enabled the detailed, systematic investigation of how temperature influences protein adsorption and denaturation (Figure 5d). It has also been possible to apply this measurement strategy to detect the washing-induced conformational changes associated with adsorbed protein aggregates as well as compare the extent of protein uptake on silica- and titania-coated sensor surfaces.

Membrane-Peptide Interactions

In addition to studying larger protein molecules, it has also been possible to utilize surface-based nanoplasmonic sensors to characterize the functional properties of shorter, amphipathic

peptides, especially in the context of membrane-peptide interactions that are related to how these peptides might be used in medical and biotechnological applications. We have primarily focused our attention on a 27-mer amphipathic, α-helical (AH) peptide that exhibits potent inhibitory activity against lipid membrane-enveloped virus particles, a process known as Lipid Envelope Antiviral Disruption (LEAD) that has been shown to work *in vivo* therapeutically.[44–46] In early work, we demonstrated that sufficiently high concentrations of AH peptide could rupture intact vesicles that were adsorbed on top of a titania-coated gold nanodisk array as well as individual vesicles on top of bare gold nanodisks.[33] Interestingly, despite a loss of lipid mass upon vesicle rupture, the LSPR measurement response was able to detect an increase in the $\Delta\lambda_{max}$ shift relative to the measurement baseline because AH peptide-induced vesicle rupture promoted a membrane structural transformation, resulting in SLB formation on the sensor surface. Lipid molecules in an SLB are, on average, in a region of higher field intensity (closer to the sensor surface) than lipid molecules in an intact vesicle, which is the reason behind the positive $\Delta\lambda_{max}$ shift.

Together with Professor Sang-Hyun Oh's group at the University of Minnesota, we also designed an EOT-based sensing platform to capture individual virus-like particles and investigate AH peptide-induced particle rupture by tracking different spectral signatures.[47] The basic design strategy involved the fabrication of a periodic array of nanoholes in a thin, gold film that was supported on a glass-based substrate; the nanohole pitch and diameter were sufficiently large to accommodate the capture of individual virus-like particles while too small for more than one particle to be captured (Figure 6a). To selectively capture particles within these nanoholes, we passivated the gold surface with a thiol-terminated polymer that inhibits particle adsorption. Thus, we were able to achieve particle adsorption into the nanoholes only, as confirmed by scanning electron microscopy (SEM) imaging (Figure 6b). When AH peptide was then added, we were able to observe the rupture of individual, virus-like particles within the nanoholes, and all three peaks in the transmission spectra shifted in response to peptide-induced particle rupture. In general, the peak positions of all three transmission maxima underwent negative $\Delta\lambda_{max}$ shifts arising from the loss of lipid mass from within the nanohole region (area of high field intensity). Interestingly, the transmission peak with the highest bulk sensitivity was least sensitive to detecting AH peptide-induced particle rupture and vice versa, highlighting how careful selection of spectral features with varying degrees of bulk and surface sensitivities is imperative for characterizing biomacromolecular interaction processes with EOT-based sensing platforms.

In related work, we have also utilized other types of nanoplasmonic sensing platforms to investigate how AH peptide preferentially targets highly curved lipid membranes.[48] On SLB-coated nanodisk arrays, the supported lipid membranes have flat configurations or present negative membrane curvature only, and AH peptide exhibited negligible binding activity to both regions (Figure 6c). In collaboration with Professor Andreas Dahlin's group at Chalmers University of Technology, we also investigated how AH peptide binds to SLB-coated nanowells that exhibit negative and positive membrane cur-
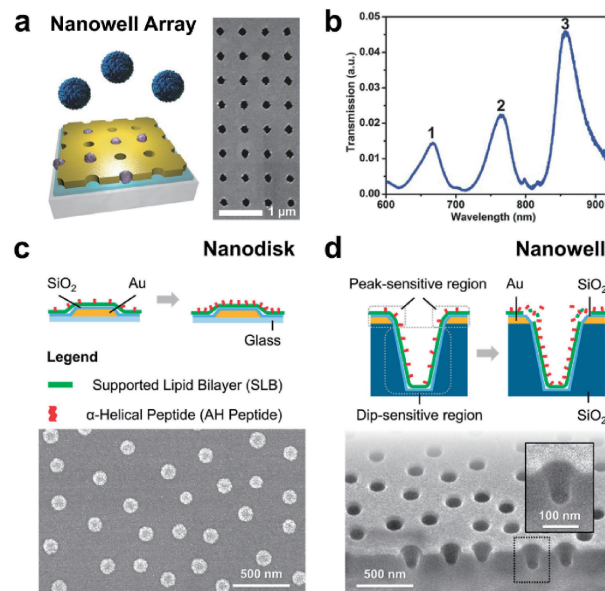

Figure 6. (a) Periodic gold nanohole array for the capture of lipid vesicles and virus particles. (b) Optical transmission spectra of a gold nanohole array in aqueous buffer solution. Reproduced from Ref. 47 with permission from Wiley-VCH, 2016. Schematic illustrations of membrane-peptide interactions with supported lipid bilayers that are conformally coated on (c) nanodisk and (d) nanowell arrays (top). Accompanying SEM micrographs of the respective sensing platforms (bottom). Reproduced from Ref. 48 with permission from American Chemical Society, 2018.

vature regions (Figure 6d). The nanowells had short-range ordering and different spectral features are known to be sensitive to the different regions of membrane curvature. The measurement results indicated large measurement responses associated with peptide binding, followed by membrane disruption, in positively curved membrane regions while there were negligible interactions with negatively curved membrane regions. Hence, the experimental findings showed that AH peptide preferentially targets positively curved membranes, which is consistent with how the peptide functions to rupture small lipid vesicles and lipid membrane-enveloped virus particles. Using similar platforms, it has also been possible to detect how certain proteins preferentially bind to negatively curved membrane regions,[49] thus demonstrating the broadly applicable measurement capabilities for addressing questions related to membrane curvature.

Combined Measurement Strategies

While surface-based nanoplasmonic sensors exhibit many competitive measurement features, integrating these sensors with other types of surface-sensitive measurement techniques can be beneficial for obtaining information about biomacromolecular interaction processes that is unobtainable from any one technique alone. Within this scope, we have investigated how a surface-based nanoplasmonic sensor based on the LSPR measurement principle can be coupled with the QCM-D technique. While LSPR measurement responses are sensitive to the

optical properties of an adsorbate (*i.e.*, biomacromolecular mass), QCM-D measurement responses are sensitive to the acoustic properties of an adsorbate (*i.e.*, biomacromolecular and hydration masses) and simultaneous monitoring of these two measurement responses can unravel insights into related factors such as hydration content within an adsorbate.

To realize such possibilities, we performed simultaneous measurements on a modified version of a QCM-D sensor chip; the substrate design included a top electrode that was coated with a silica spacer layer on which randomly distributed gold nanodisks were fabricated and the entire surface was then sputter-coated with a thin layer of oxide material. The sensor chips were placed in a microfluidic flow cell that is commonly used for QCM-D measurements, with one special feature: a transparent glass window on top to facilitate light transmission. An optical fiber probe was also integrated together with the flow cell so that the measurement chamber was connected with both the light source and spectrophotometer for LSPR measurements along with the electronics unit for QCM-D measurements (Figure 7a). The optical fiber probe illuminated the top of the sensor chip through the window and the nanoplasmonic sensing measurements were conducted in reflection mode (Figure 7b). In this configuration, LSPR and QCM-D measurements can be tracked simultaneously on the same sensor surface.

Using this combined setup, we followed AH peptide-induced vesicle rupture and SLB formation on a titania-coated surface.[50] Interestingly, when AH peptide was added to rupture adsorbed, intact vesicles on the sensor surface, the QCM-D response indicated a net decrease in acoustic mass while the LSPR measurement response showed a net increase in optical mass (Figures 7c–d). This distinction could be explained, and built upon, by considering the detection principles behind optical versus acoustic mass measurements along with accounting for the different surface sensitivities of the two measurement techniques. By tracking these measurement responses as a function of time, it was possible to temporally unravel different stages of the AH peptide-induced vesicle rupture and SLB formation processes (Figure 7e). These measurement capabilities have also been utilized to investigate the effects of vesicle size on the adsorption behavior of lipid vesicles on titania surfaces.[51] It was found that, with increasing vesicle size, adsorbing vesicles underwent greater deformation, however, the packing efficiency became lower due to steric effects. Thus, intermediate vesicle sizes (around 130–150 nm diameter) were optimal for forming well-packed adlayers and demonstrate how the combined measurement strategy could decouple competing factors involved in biomacromolecular interaction processes.

Outlook

As discussed in this Account, our team and many other research groups around the world have been exploring surface-based nanoplasmonic sensors for biointerfacial science applications. While we have primarily focused on fundamental science topics, there are untapped opportunities to apply these measurement capabilities, especially within the scope of the INPS concept, for translational applications, such as clinical diagnostics. For example, surface-based nanoplasmonic sensors could be useful for detecting cancer biomarkers such as
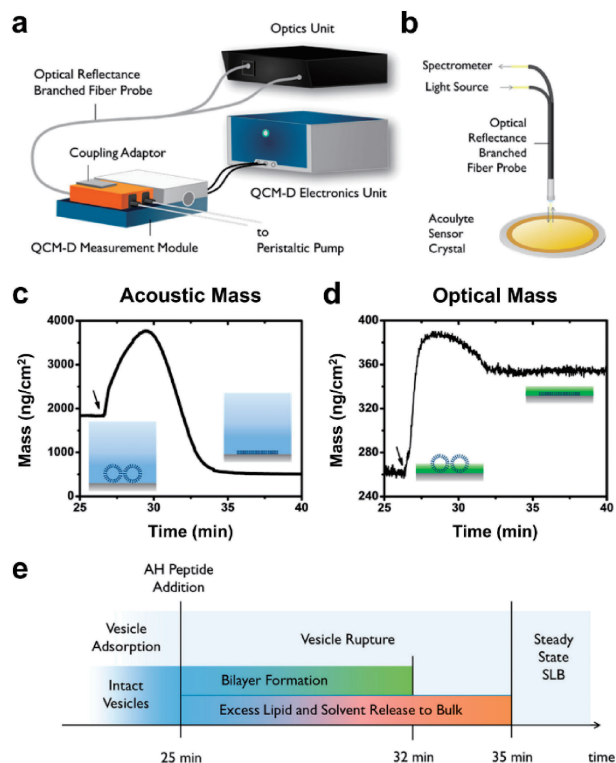

Figure 7. (a) Schematic illustration of the combined LSPR and QCM-D instrument setup. (b) Operating principles behind the reflection-based LSPR measurement configuration. (c) Time-dependent variation in the acoustic mass as determined by analysis of the QCM-D measurement data. (d) Time-dependent variation in the optical mass as determined by analysis of the LSPR measurement data. (e) Summary of the stages involved in the biomacromolecular interaction process, including vesicle rupture, supported lipid bilayer formation, and release of excess lipid molecules, as determined by combined LSPR and QCM-D measurement analysis. Reproduced from Ref. 50 with permission from American Chemical Society, 2016.

circulating nucleic acid strands and circulating tumor cells.[52] Ultimately, realizing the full potential of surface-based nanoplasmonic sensors will require establishing robust fabrication strategies along with deeply understanding how sensor design aspects are linked to analytical performance. With so many design possibilities, it will be important to explore different options while also working towards standardized platforms that can be used by researchers worldwide and thus set universal measurement standards for comparing experimental data and generating new insights into biomacromolecular interaction processes from fundamental and applied perspectives. Looking forward, there is excellent potential to continue developing surface-based nanoplasmonic sensors for biointerfacial science applications, and these capabilities can lead to significant chemical insights along with providing new measurement tools for medicine, biotechnology, and environmental science among many other fields.

References

1   J. Lafait, S. Berthier, C. Andraud, V. Reillon, J. Boulenguez, *C. R. Phys.* **2009**, *10*, 649.

2   J. Ueda, M. Samusawa, K. Kumagai, A. Ishida, S. Tanabe, *J. Mater. Sci.* **2014**, *49*, 3299.

3   K. A. Willets, R. P. Van Duyne, *Annu. Rev. Phys. Chem.* **2007**, *58*, 267.

4   J. N. Anker, W. P. Hall, O. Lyandres, N. C. Shah, J. Zhao, R. P. Van Duyne, *Nat. Mater.* **2008**, *7*, 442.

5   M. I. Stockman, *Opt. Express* **2011**, *19*, 22029.

6   M. I. Stockman, *Phys. Today* **2011**, *64*, 39.

7   N. C. Lindquist, P. Nagpal, K. M. McPeak, D. J. Norris, S.-H. Oh, *Rep. Prog. Phys.* **2012**, *75*, 036501.

8   K. Ariga, Q. Ji, W. Nakanishi, J. P. Hill, M. Aono, *Mater. Horiz.* **2015**, *2*, 406.

9   A. B. Dahlin, N. J. Wittenberg, F. Höök, S.-H. Oh, *Nanophotonics* **2013**, *2*, 83.

10   B. Špačková, P. Wrobel, M. Bocková, J. Homola, *Proc. IEEE* **2016**, *104*, 2380.

11   J. A. Jackman, A. R. Ferhan, N.-J. Cho, *Chem. Soc. Rev.* **2017**, *46*, 3615.

12   G. A. Lopez, M.-C. Estevez, M. Soler, L. M. Lechuga, *Nanophotonics* **2017**, *6*, 123.

13   R. G. Freeman, K. C. Grabar, K. J. Allison, R. M. Bright, J. A. Davis, A. P. Guthrie, M. B. Hommer, M. A. Jackson, P. C. Smith, D. G. Walter, M. J. Natan, *Science* **1995**, *267*, 1629.

14   M.-C. Daniel, D. Astruc, *Chem. Rev.* **2004**, *104*, 293.

15   S. Unser, I. Bruzas, J. He, L. Sagle, *Sensors* **2015**, *15*, 15684.

16   J. Li, C. Chen, L. Lagae, P. Van Dorpe, *J. Phys. Chem. C* **2015**, *119*, 29116.

17   F. Mazzotta, T. W. Johnson, A. B. Dahlin, J. Shaver, S.-H. Oh, F. Höök, *ACS Photonics* **2015**, *2*, 256.

18   J. Li, J. Ye, C. Chen, Y. Li, N. Verellen, V. V. Moshchalkov, L. Lagae, P. Van Dorpe, *ACS Photonics* **2015**, *2*, 425.

19   S.-H. Oh, H. Altug, *Nat. Commun.* **2018**, *9*, 5263.

20   T. W. Ebbesen, H. J. Lezec, H. F. Ghaemi, T. Thio, P. A. Wolff, *Nature* **1998**, *391*, 667.

21   L. Martín-Moreno, F. J. García-Vidal, H. J. Lezec, K. M. Pellerin, T. Thio, J. B. Pendry, T. W. Ebbesen, *Phys. Rev. Lett.* **2001**, *86*, 1114.

22   H. Im, S. H. Lee, N. J. Wittenberg, T. W. Johnson, N. C. Lindquist, P. Nagpal, D. J. Norris, S.-H. Oh, *ACS Nano* **2011**, *5*, 6244.

23   H. Im, H. Shao, Y. I. Park, V. M. Peterson, C. M. Castro, R. Weissleder, H. Lee, *Nat. Biotechnol.* **2014**, *32*, 490.

24   T. Rindzevicius, Y. Alaverdyan, A. Dahlin, F. Höök, D. S. Sutherland, M. Käll, *Nano Lett.* **2005**, *5*, 2335.

25   T. Sannomiya, O. Scholder, K. Jefimovs, C. Hafner, A. B. Dahlin, *Small* **2011**, *7*, 1653.

26   C. Langhammer, E. M. Larsson, B. Kasemo, I. Zorić, *Nano Lett.* **2010**, *10*, 3529.

27   E. M. Larsson, M. E. Edvardsson, C. Langhammer, I. Zorić, B. Kasemo, *Rev. Sci. Instrum.* **2009**, *80*, 125105.

28   E. M. Larsson, S. Syrenova, C. Langhammer, *Nanophotonics* **2012**, *1*, 249.

29   W. P. Hall, J. Modica, J. Anker, Y. Lin, M. Mrksich, R. P. Van Duyne, *Nano Lett.* **2011**, *11*, 1098.

30   M. P. Jonsson, P. Jönsson, A. B. Dahlin, F. Höök, *Nano Lett.* **2007**, *7*, 3462.

31   M. Svedendahl, S. Chen, A. Dmitriev, M. Käll, *Nano Lett.* **2009**, *9*, 4428.

32   K. M. Mayer, J. H. Hafner, *Chem. Rev.* **2011**, *111*, 3828.

33   G. H. Zan, J. A. Jackman, S.-O. Kim, N.-J. Cho, *Small* **2014**, *10*, 4828.

34   J. A. Jackman, V. P. Zhdanov, N.-J. Cho, *Langmuir* **2014**, *30*, 9494.

35   M. Dacic, J. A. Jackman, S. Yorulmaz, V. P. Zhdanov, B. Kasemo, N.-J. Cho, *Langmuir* **2016**, *32*, 6486.

36   J. A. Jackman, B. Špačková, E. Linardy, M. C. Kim, B. K. Yoon, J. Homola, N.-J. Cho, *Chem. Commun.* **2016**, *52*, 76.

37   J. A. Jackman, S. Y. Avsar, A. R. Ferhan, D. Li, J. H. Park, V. P. Zhdanov, N.-J. Cho, *Anal. Chem.* **2017**, *89*, 1102.

38   E. Oh, J. A. Jackman, S. Yorulmaz, V. P. Zhdanov, H. Lee, N.-J. Cho, *Langmuir* **2015**, *31*, 771.

39   A. R. Ferhan, J. A. Jackman, N.-J. Cho, *Anal. Chem.* **2017**, *89*, 4301.

40   A. R. Ferhan, B. Špačková, J. A. Jackman, G. J. Ma, T. N. Sut, J. Homola, N.-J. Cho, *Anal. Chem.* **2018**, *90*, 12503.

41   A. R. Ferhan, G. J. Ma, J. A. Jackman, T. N. Sut, J. H. Park, N.-J. Cho, *Sensors* **2017**, *17*, 1484.

42   J. A. Jackman, A. R. Ferhan, B. K. Yoon, J. H. Park, V. P. Zhdanov, N.-J. Cho, *Anal. Chem.* **2017**, *89*, 12976.

43   J. H. Park, J. A. Jackman, A. R. Ferhan, G. J. Ma, B. K. Yoon, N.-J. Cho, *ACS Appl. Mater. Interfaces* **2018**, *10*, 32047.

44   J. A. Jackman, H. Z. Goh, V. P. Zhdanov, W. Knoll, N.-J. Cho, *J. Am. Chem. Soc.* **2016**, *138*, 1406.

45   J. A. Jackman, V. V. Costa, S. Park, A. L. C. V. Real, J. H. Park, P. L. Cardozo, A. R. Ferhan, I. G. Olmo, T. P. Moreira, J. L. Bambirra, V. F. Queiroz, C. M. Queiroz-Junior, G. Foureaux, D. G. Souza, F. M. Ribeiro, B. K. Yoon, E. Wynendaele, B. De Spiegeleer, M. M. Teixeira, N.-J. Cho, *Nat. Mater.* **2018**, *17*, 971.

46   J. A. Jackman, P.-Y. Shi, N.-J. Cho, *ACS Infect. Dis.* **2019**, *5*, 4.

47   J. A. Jackman, E. Linardy, D. Yoo, J. Seo, W. B. Ng, D. J. Klemme, N. J. Wittenberg, S.-H. Oh, N.-J. Cho, *Small* **2016**, *12*, 1159.

48   A. R. Ferhan, J. A. Jackman, B. Malekian, K. Xiong, G. Emilsson, S. Park, A. B. Dahlin, N.-J. Cho, *Anal. Chem.* **2018**, *90*, 7458.

49   G. Emilsson, E. Röder, B. Malekian, K. Xiong, J. Manzi, F.-C. Tsai, N.-J. Cho, M. Bally, A. Dahlin, *Front Chem.* **2019**, *7*. doi:10.3389/fchem.2019.00001.

50   A. R. Ferhan, J. A. Jackman, N.-J. Cho, *Anal. Chem.* **2016**, *88*, 12524.

51   A. R. Ferhan, J. A. Jackman, N.-J. Cho, *Phys. Chem. Chem. Phys.* **2017**, *19*, 2131.

52   A. R. Ferhan, J. A. Jackman, J. H. Park, N.-J. Cho, D.-H. Kim, *Adv. Drug Delivery Rev.* **2018**, *125*, 48.